Modeling Erbium-Doped Fiber Amplifiers

C. Randy Giles, *Member, IEEE*, and Emmanuel Desurvire, *Member, IEEE*

(Invited Paper)

Abstract—**Erbium-doped fiber amplifiers are modeled using the propagation and rate equations of a homogeneous, two-level laser medium. Numerical methods are used to analyze the effects of optical modes and erbium confinement on amplifier performance, and to calculate both the gain and ASE spectra. Fibers with confined erbium doping are completely characterized from easily measured parameters: the ratio of the linear ion density to fluorescence lifetime, and the absorption of gain spectra. Then analytical techniques allow accurate evaluation of gain, saturation, and noise in low-gain amplifiers** ($G \leq$ 20 dB).

I. Introduction

THE development of erbium-doped glass fibers has been a major impetus to research on active-fiber technology in the 1.55-μm wavelength region. After the pioneering work on fiber lasers [1], [2], research on rare-earth doped-fibers remained nearly dormant until the demonstration of high-gain erbium-doped fiber amplifiers [3], [4], and their use in lightwave transmission systems [5], [6]. Now these active fibers are finding diverse applications in optical amplifiers, lasers, switches, and a variety of nonlinear devices.

Some of the notable results achieved with erbium-doped fiber amplifiers are 51-dB optical gain [7], 100-mW saturated output power [8], and 3-dB noise figure [9]. Such high-performance amplifiers may enhance lightwave systems and have already been used to achieve numerous transmission records [10]–[12]. Erbium-doped fibers also have had a major impact in fiber lasers and superfluorescent light sources. Here, recent achievements include 71% pumping efficiency [13], 60-kHz laser linewidth [14], and passive mode-locking of a fiber laser [15]. Finally, several experiments on optical switching and optical nonlinearities [16], [17] highlight the potential of rare-earth doped fiber in future photonic systems or instrumentation.

Concurrent with these experiments, amplifier and laser models based on rate and propagation equations have appeared in the literature. These models are important for predicting amplifier and laser behavior, and for yielding improved fiber designs. Although all these models originate from the same basic equations, each is tailored for a specific problem. For example, rather than resolve the amplified spontaneous emission (ASE) spectrum, several amplifier models replace it with an equivalent noise bandwidth [18]–[21]. Models are also simplified by replacing transverse space integrals in the propagation equation with an effective overlap parameter. Here, we examine these types of approximations while developing several of the commonly used amplifier models. Although only amplifier models are discussed in this paper, laser and optical-switch problems can often be solved with slight changes to the amplifier equations.

In Section II, we briefly comment on the spectroscopic properties of the erbium in glass. The rate equations for the ion population distribution and the propagation equations are introduced in Section III. The rest of the paper is devoted to analyzing specific models. These models are presented in order of diminishing complexity. Sections IV and V describe numerical models that simulate the guided modes and ASE spectrum, respectively. Following the numerical models, several analytical models derived from simplified rate and propagation equations, are presented in Sections VI–VIII. Within the constraints of their approximations, these analytical models appear to be accurate and provide considerable insight into characteristics such as the length dependence of amplifier gain and the spectral dependence of noise and gain saturation.

II. Properties of Erbium in Glass

The absorption and emission spectra of the Er^{3+} ion are signatures of the energy states of its $4f$ inner electrons. In a glass or crystal host, these energy states are modified by local electric fields that cause Stark-splitting and by dynamical perturbation, i.e., "thermal" or homogeneous broadening [22]–[24]. Inhomogeneous broadening results from the structural disorder of the glass that causes differences in the electric fields at various sites. Other dopants added to the glass may alter these effects. Rare-earth ions in silicate glasses are too large to occupy interstitial sites and are more easily incorporated into the glass structure by adding a network modifier such as Al, to produce unbridged oxygen to which the rare earth attaches. With the silicate glass already composed of a random network of SiO_4 tetrahedra, this multicomponent glass adds more coordination possibilities at sites and larger variation in the bonding distances. This changes the Stark-splitting and enhances the inhomogeneity of the gain medium.

The energy level diagram of Fig. 1 summarizes typical homogeneous and inhomogeneous linewidths associated with $^4I_{11/2}$, $^4I_{13/2}$, and $^4I_{15/2}$ levels of Er^{3+} in silicate glass. The $^4I_{11/2}$–$^4I_{15/2}$ transition corresponds to the 980-nm pump band and the $^4I_{13/2}$–$^4I_{15/2}$ transition corresponds to the 1520–1570-nm signal band and the resonant pumping in the 1460–1500-nm band. Other pump bands, and the potential for more complex phenomena such as, pump excited-state absorption (ESA), are associated with other energy levels of Er^{3+}, but were not included in the figure. No ESA occurs for 980-nm or 1480-nm pumped amplifiers. The Stark levels appear as hatched bars to indicate the Boltzmann-distributed occupancy of each level within the manifold. Temperature changes alter the population of each level and consequently alter the absorption and emission spectra. For example, at temperatures close to 0°K, only the

Manuscript received October 12, 1990; revised November 8, 1990.

The authors are with AT&T Bell Laboratories, Crawford Hill Laboratory, Holmdel, NJ 07733.

IEEE Log Number 9041692.

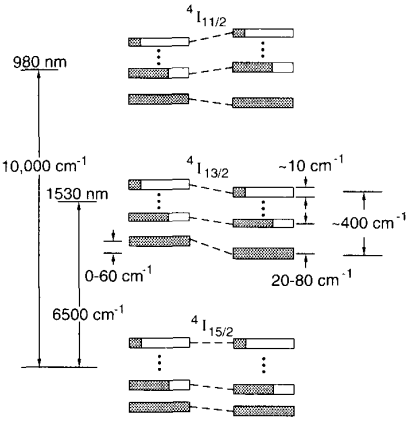

Fig. 1. Energy level diagram of Er^{3+} in silicate glasses showing homogeneous and inhomogeneous broadening of the Stark-split levels. Shading represents room-temperature Boltzmann-distributed population of each manifold.

lowest level of each manifold is occupied. Then the $^4I_{13/2}$–$^4I_{15/2}$ absorption and emission spectra correspond to the inhomogeneously broadened Stark levels of the $^4I_{13/2}$ and $^4I_{15/2}$ manifolds, respectively.

Two examples of the room-temperature absorption and stimulated emission spectra obtained from erbium-doped silica glass fibers are shown in Fig. 2. The fiber of Fig. 2(a) had only germanium as an index-raising codopant while the fiber of Fig. 2(b) had aluminum added to improve the solubility of the Er^{3+} in glass. Adding Al also broadens the amplifier gain spectrum. The left y axis of the figures is the loss (gain) per meter of fiber and the right axis is the absorption (emission) cross section. The loss spectra are measured using a white-light source and monochromator. The gain spectra are measured with a large pump power at 980 or 528 nm to fully invert the Er^{3+} population to the $^4I_{13/2}$ energy level. Then the measured loss spectrum $\alpha(\lambda)$ and gain spectrum $g^*(\lambda)$ are

$$\alpha(\lambda) = \sigma_a(\lambda)\Gamma(\lambda)n_t$$
$$g^*(\lambda) = \sigma_e(\lambda)\Gamma(\lambda)n_t \qquad (1)$$

where $\Gamma(\lambda)$ is the overlap integral between the optical mode and the erbium ions and n_t is the density of erbium ions. The absorption and emission cross sections are $\sigma_a(\lambda)$ and $\sigma_s(\lambda)$, respectively.

One of the difficulties in characterizing erbium-doped fibers has been to accurately measure $\sigma_a(\lambda)$ and $\sigma_e(\lambda)$. In bulk glass samples, analytical chemistry methods can be used to determine n_t and the spectra are measured with large optical beams where $\Gamma = 1$. Then $\alpha_a(\lambda)$ and $\sigma_e(\lambda)$ are obtained directly. This method cannot be used with fibers where n_t varies radially and Γ is not well-known. Instead, the cross sections are obtained indirectly, often with the Ladenburg–Fuchbauer (LF) equation, which calculates the peak cross section from integrated spectrum [25], [26]. One form of this equation is

$$\sigma_{a,e}(\lambda) = \frac{\lambda^4_{a,e,peak} I_{a,e}(\lambda)}{8\pi c n^2 \tau \int I_{a,e}(\lambda)\, d\lambda} \qquad (2)$$

where $\lambda_{a,e,peak}$ is the wavelength at the absorption (emission) peak, τ is the lifetime of the metastable level, n is the refractive

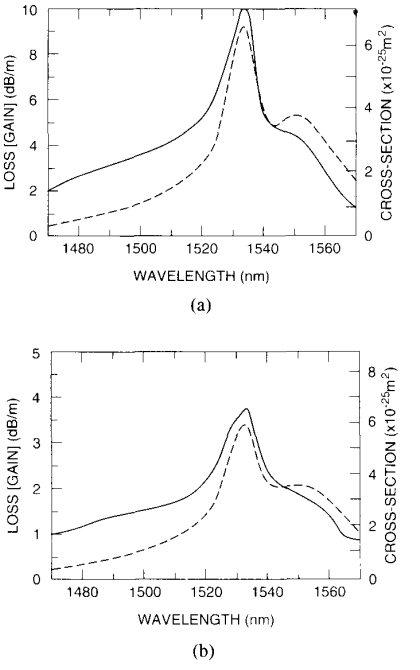

Fig. 2. Absorption (——) and gain (- - -) spectra of (a) Ge : silicate and (b) Al : Ge : silicate amplifier fibers. Cross section calculated from Ladenburg-Fuchbauer equation is shown on right axis.

index of the glass, c is the velocity of light, and $I_{a,e}(\lambda)$ the absorption or fluorescence spectrum. Equation (2) was used to calculate the cross-section values in Fig. 2. However, cross-section values obtained from the LF relation are not very accurate [26]. It is better, if possible, to use the directly measured quantities $\alpha(\lambda)$ and $g^*(\lambda)$ as model parameters. This is done for most of the models discussed here.

Measurement of only absorption and emission spectra does not establish the relative contributions of homogeneous and inhomogeneous broadening to the observed linewidth. This is important to know because it may significantly affect the pumping and saturation behavior of the amplifier. For example, some ions may have a smaller absorption cross section at the pump wavelength and inversion of the whole population requires more pump power. Similarly, large-signal gain saturation is more gradual because of the site-dependent emission cross sections of the erbium ion. Generally then, the observed cross-section spectra $\sigma_{a,e}(\nu)$ are the convolution of homogeneous cross section $\sigma^h_{a,e}(\nu)$ with the probability distribution $f(\nu)$ of the transition wavelength fluctuations caused by inhomogeneous broadening, i.e.,

$$\sigma_{a,e}(\nu) = \int_{-\infty}^{\infty} \sigma^h_{a,e}(\nu')\, f(\nu - \nu')\, d\nu'. \qquad (3)$$

The well-established techniques of fluorescence line narrowing and spectral hole broadening [27], [28], have recently been applied to erbium-doped glasses and fibers to resolve the homogeneous and inhomogeneous linewidths [29]–[31]. Measurements of alumino-silicate and fluoride glasses have shown the inhomogeneous linewidth to be comparable to or less than the homogeneous line broadening. Germano-silicate glasses, appear to have greater inhomogeneous linewidths (~ 8

nm) than the room temperature homogeneous linewidth (3–4 nm). Recent study which compared a homogeneous description to an inhomogeneous description based on (3), indicates that gain saturation in alumino-silicate glasses can be modeled to be homogeneous [32]. This is less certain for some glasses, including the germano-silicate glass, and more study is needed. However, many experiments using both alumino-silicate and germano-silicate fibers have been successfully explained with homogeneous models. In the rest of this paper, we will consider only homogeneous gain effects.

Lastly, we justify the two-level model of the amplifier gain medium. For pumping into the 980-nm absorption band, this implies that the population in the $^4I_{11/2}$ manifold is negligible. This depletion of the pump level is nominally satisfied when the nonradiative decay rate from the pump level W_{nr} is much larger than the pumping rate $W_{\text{pump}} = P_p\sigma_{ap}/h\nu_p A$ where P_p is the pump power, ν_p is the pump frequency, and A is the mode area. For typical fiber amplifier parameters, treating the 980-nm pumped amplifier with a two-level model is valid for average pump powers less than 1 W; this is satisfied in all reported fiber amplifier experiments. Although W_{nr} increases exponentially with the energy gap between levels [33], the two-level model can be used for short wavelength pumps, e.g., 800 and 670 nm, because the nonradiative decay is a fast process passing through intermediate levels to fill the $^4I_{13/2}$ metastable level. Finally, direct pumping into the $^4I_{13/2}$–$^4I_{15/2}$ transition also behaves as a two-level system because of the rapid thermalization in the metastable manifold.

III. Propagation and Rate Equation

Models of homogeneously broadened two-level systems are useful for fiber amplifiers pumped in the 1480- and 980-nm absorption bands. Additional equations are needed for more complex models incorporating effects such as pump excited-state absorption, energy transfer between ions, or inhomogeneous broadening. However, because the methods of solution are similar for all these cases, the examples here are restricted to the two-level model. Then it is easier to validate approximations to the overlap integral and the effective ASE bandwidth, and to compare the numerical and analytical models.

We can think of light in the amplifier to be propagating as a number of optical beams of frequency bandwidth $\Delta\nu_k$ centered at the optical wavelength $\lambda_k = c/\nu_k$. This notation describes both narrow line beams such as pump and signal sources when $\Delta\nu_k \doteq 0$, and broadband ASE where $\Delta\nu_k$ equals the frequency steps used in the simulation to resolve the ASE spectrum. Then integration over optical frequency is approximated by a summation over k. Integrating the light intensity distribution of the kth beam $I_k(r, \phi, z)$ over the radial and azimuthal coordinates gives the beam's total power $P_k(z)$ at position z in the fiber amplifier

$$P_k(z) = \int_0^{2\pi}\int_0^{\infty} I_k(r, \phi, z) r\, dr\, d\phi. \tag{4}$$

The normalized optical intensity is defined as

$$i_k(r, \phi) = I_k(r, \phi, z)/P_k(z). \tag{5}$$

Here we assumed that $I_k(r, \phi, z)$ is separable such that the shape of the kth optical mode is independent of z.

Rate equations describe the effects of absorption, stimulated emission, and spontaneous emission on the populations of the ground and metastable states. For this two-level system with the k optical beams

$$\frac{dn_2}{dt} = \sum_k \frac{P_k i_k \sigma_{ak}}{h\nu_k} n_1(r, \phi, z) - \sum_k \frac{P_k i_k \sigma_{ek}}{h\nu_k} n_2(r, \phi, z) - \frac{n_2(r, \phi, z)}{\tau} \tag{6}$$

$$n_t(r, \phi, z) = n_1(r, \phi, z) + n_2(r, \phi, z). \tag{7}$$

Equation (7) is the particle conservation for the two level system, where $n_t(r, \phi, z)$ is the local erbium ion density.

The remaining equations describe the propagation of the beams through the fiber, i.e.,

$$\frac{dP_k}{dz} = u_k\sigma_{ek}\int_0^{2\pi}\int_0^{\infty} i_k(r, \phi) n_2(r, \phi, z) r\, dr\, d\phi \left(P_k(z) + mh\nu_k\Delta\nu_k\right) - u_k\sigma_{ak}\int_0^{2\pi}\int_0^{\infty} i_k(r, \phi) \cdot n_1(r, \phi, z) r\, dr\, d\phi \left(P_k(z)\right) \tag{8}$$

where each beam is traveling either in the forward ($u_k = 1$) or backward ($u_k = -1$) direction. Here $mh\nu_k\Delta\nu_k$ is the contribution of spontaneous emission from the local n_2 population, and its growth through the amplifier. In models that have ASE, both the forward and backward components should be included. The number of modes m is normally 2, as in the case of the optical fiber supporting only the two polarization states of the lowest order optical mode.

Once the boundary conditions for the k beams are specified at $z = 0, L$, (6) and (8) are integrated over space (z), optical frequency (k), and time (t). By setting the time derivative in (6) equal to zero, the problem is reduced to the steady-state case. This condition is applicable for CW beams, or those modulated at frequencies greater than ~10 kHz [34], [35]. In Section VIII, small-signal analysis is used to establish the validity of CW models.

Several steady-state models are examined here, as shown in the tree diagram of Fig. 3. The diagram branches between models that include the radial optical and erbium distributions, and those that utilize an effective overlap integral. Using the effective overlap integral greatly reduces the computational effort, but assumes the special condition that the erbium is confined to the center of the optical mode. Otherwise, arbitrary dopant distributions are analyzed using spatial models. Spatial models are used to optimize the fiber waveguide and dopant distribution.

Branching occurs between models that include ASE and those that ignore it. ASE terms are required for calculating amplifier noise and gain saturation caused by ASE. In some cases the ASE might be modeled as optical power in an effective noise bandwidth $\Delta\nu_{\text{eff}}$. Although the noise bandwidth changes with inversion, error from using $\Delta\nu_{\text{eff}}$ is minimized by establishing *a priori*, a bandwidth corresponding to the operating point. Otherwise, the full ASE spectrum should be resolved.

IV. Spatial-Mode Modeling in Erbium Amplifiers

A good amplifier should have high efficiency, low noise, and a low pump threshold. Among the factors affecting these are the spatial modes of the pump and signal light, and the distribution of the erbium ions. Small mode sizes obviously help to reduce the pump power needed to achieve gain. Lower pump thresh-

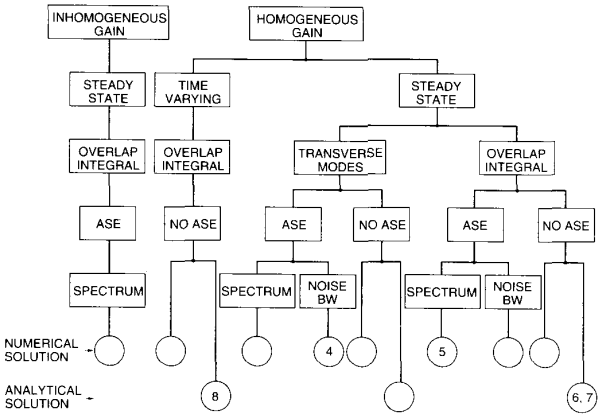

Fig. 3. Tree diagram showing relationships among existing amplifier models. Numbers indicate sections in this paper describing the numerical or analytical model.

olds are also obtained by confining the erbium to the center portion of the optical modes where the intensities are highest and pumping is most efficient.

Here we examine fiber design using a step approximation to the core-index profile and a weakly guided approximation for the optical-mode distribution [36]. Then the normalized intensity distribution of the fundamental mode (LP_{01}) for a fiber having core radius a core index n_{core}, and cladding index n_{clad} is

$$i(r) = \frac{1}{\pi}\left[\frac{v}{aV}\frac{J_0(ur/a)}{J_1(u)}\right]^2 \quad r < a$$

$$= \frac{1}{\pi}\left[\frac{u}{aV}\frac{K_0(vr/a)}{K_1(v)}\right]^2 \quad r \geq a \tag{9}$$

where $J_{0,1}$ and $K_{0,1}$ are the Bessel and modified Bessel functions, respectively. The fiber V number is $2\pi a/\lambda_k\ (n_{\text{core}}^2 - n_{\text{clad}}^2)^{1/2}$ and the variables u and v come from matching the solutions at $r = a$; for $1 \leq V \leq 3$, we use the approximation $v = 1.1428V - 0.9960$, $u = (V^2 - v^2)^{1/2}$ [37]. Obviously, the model can be extended to the superposition of several optical modes, to describe for example, a core that is underpumped by an LP_{11} pump mode [38], [39]. Most amplifier fibers support only the fundamental modes of the pump and signal except possibly for very short wavelength pump wavelengths, e.g., 670 and 532 nm. Then it is difficult to have a fiber whose cutoff wavelength is below the pump wavelength and still guide at the signal wavelength, $\lambda_s \sim$ 1520–1560 nm.

Two principal fiber characteristics are α_k and g_k^*, the fiber absorption and gain spectra, respectively. Expressed in terms of distributions of the ions and optical modes, these quantities are

$$\alpha_k = \sigma_{ak}\int_0^{2\pi}\int_0^{\infty} i_k(r, \phi)\, n_t(r, \phi, z) r\, dr\, d\phi$$

$$g_k^* = \sigma_{ek}\int_0^{2\pi}\int_0^{\infty} i_k(r, \phi) n_t(r, \phi, z) r\, dr\, d\phi. \tag{10}$$

If the erbium ions are uniformly distributed in a disk of radius b, concentric with the fiber core a_k and g_k^* are

$$\alpha_k = \sigma_{ak}\Gamma_k n_t$$

$$g_k^* = \sigma_{ek}\Gamma_k n_t \tag{11}$$

where the overlap integral between the dopant and optical mode Γ_k is

$$\Gamma_k = \int_0^{2\pi}\int_0^{b} i_k(r, \phi) r\, dr\, d\phi. \tag{12}$$

Written in terms of these new parameters, the amplifier propagation equation becomes

$$\frac{dP_k}{dz} = \frac{\alpha_k + g_k^*}{\Gamma_k} P_k \int_0^{2\pi}\int_0^{b} \frac{n_2(r, \phi, z)}{n_t} i_k r\, dr\, d\phi - (\alpha_k + l_k)P_k$$

$$+ \frac{g_k^*}{\Gamma_k} mh\nu_k \Delta\nu_k \int_0^{2\pi}\int_0^{b} \frac{n_2(r, \phi, z)}{n_t} i_k r\, dr\, d\phi. \tag{13}$$

An additional loss term l_k has been added to the propagation equation to account for excess fiber loss. This loss can be significant in fibers having high water content, scattering from devitrification in high-index cores, or in fibers that are lightly doped for use as distributed amplifiers [40]. If $n_2 = 0$, the propagation equation reduces to that of exponential attenuation at a loss rate $a_k + l_k$; complete inversion has $n_2 = n_t$, then the gain exponent is $g_k^* - l_k$.

The set of equations is closed with the steady-state approximation to the metastable population, which from (6) is

$$n_2(r, \phi, z) = n_t \frac{\sum_k \frac{\tau\sigma_{ak}}{h\nu_k} P_k i_k}{1 + \sum_k \tau \frac{(\sigma_{ak} + \sigma_{ek})}{h\nu_k} P_k i_k}. \tag{14}$$

Solutions to (13) and (14) are obtained by standard numerical integration techniques. If ASE is small and not included, then coupled propagation equations for the pump and signal beams are integrated with the noise source terms set to zero. By employing an effective noise bandwidth $\Delta\nu_k$, propagation equations for the forward and backward ASE can be added; typical values of $\Delta\nu_k$ are 200–2000 GHz, depending upon the fiber composition and operating conditions. The noise bandwidth may be estimated from, $\Delta\nu_k = \int_0^{\infty} (\sigma_e(\nu)/\sigma_{e,peak})\, d\nu$, but can be unreliable where the bandwidth changes rapidly with pump or signal power. This can occur for highly efficient amplifiers having low threshold pump powers or in very high-gain amplifiers. Then the problem should be solved for a large number of k to adequately resolve the ASE spectrum.

As an example, Fig. 4 shows the signal gain, gain coefficient (G/P_p), pump absorption, and ASE powers calculated for a high-efficiency amplifier fiber having a 1.2-μm index core radius and index step of 0.035. The noise and signal were centered about 1550 nm and the pump wavelength was 1480 nm. The rest of the fiber amplifier parameters, listed in Table I for a fiber with Er radius $b = 1.2$ μm, are similar to those of a recently reported high-efficiency amplifier [41]. The noise bandwidth was estimated to be 1250 GHz (10 nm). Calculations were made for three values of b values to illustrate the importance of obtaining localized erbium doping. The values of α_p and g_p^*, were scaled as functions of b to properly account for changes in the pump and signal overlap integrals. In the case of the uniformly doped core $a = b = 1.2$ μm, and $\Gamma_p = 0.62$, $\Gamma_s = 0.58$.

As expected, higher confinement of the erbium yields lower pump thresholds for transparency and higher gain coefficients. The peak-gain coefficient, 8.1 dB/mW for $b = 0.6$ μm at 1480 nm, may be difficult to achieve in small-core fibers because of

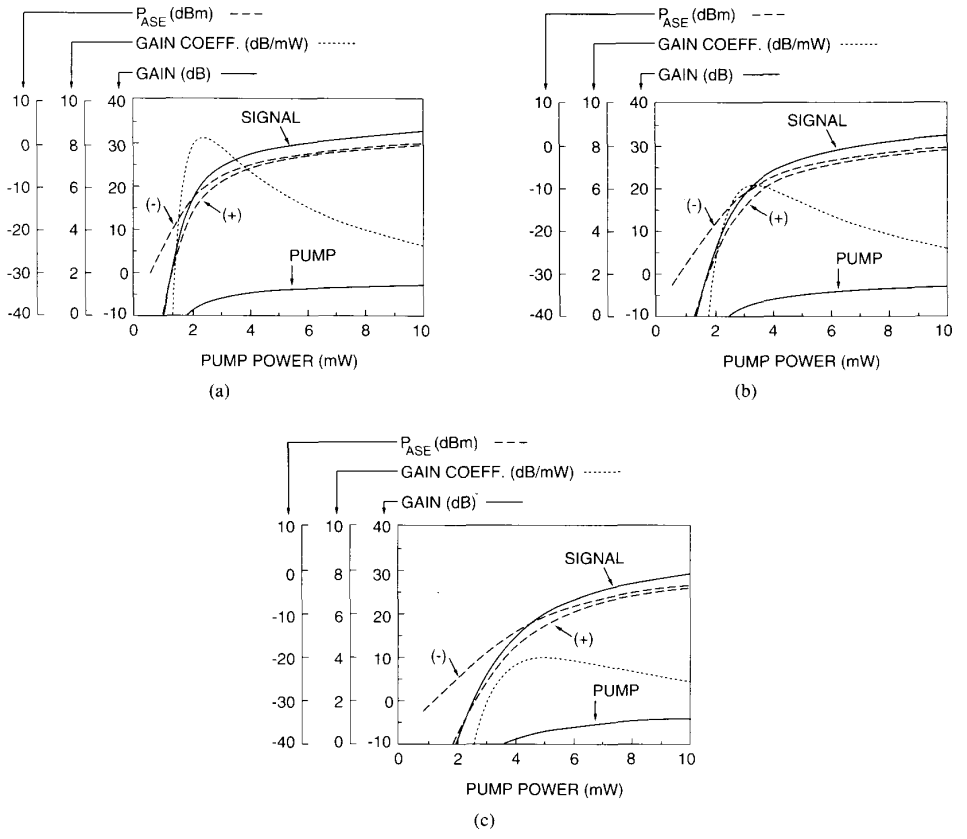

Fig. 4. Amplifier gain, gain coefficient, and ASE power versus pump power for an Al-silicate, Er^{3+}-doped fiber amplifier (parameters listed in Table I). Calculated from spatial model with uniformly doped Er^{3+} core radius of (a) 0.6 μm, (b) 1.2 μm, and (c) 1.8 μm.

TABLE I
FIBER PARAMETERS USED IN SPATIAL MODEL (FIGS. 4 AND 5)

Index core radius	$a = 1.2\ \mu m$	Amplifier length	$L = 18.8$ m
Index step	$\Delta n = 0.035$	Metastable lifetime	$\tau = 10$ ms
Er^{3+} core radius	$b = 1.2\ \mu m$	ASE bandwidth	$\Delta\lambda_{ASE} = 10$ nm (Fig. 4) $= 0$ nm (Fig. 5)
	Pump		Signal
Wavelength:	$\lambda_p = 1480$ nm		$\lambda_s = 1550$ nm
Absorption coeff.	$\alpha_p = 1.6$ dB/m		$\alpha_s = 2.6$ dB/m
Gain coeff.	$g_p^* = 0.5$ dB/m		$g_s^* = 3.6$ dB/m
Excess loss	$l_p = 0.03$ dB/m (Fig. 4) $= 0$ dB/m (Fig. 5)		$l_s = 0.03$ dB/m (Fig. 4) $= 0$ dB/m (Fig. 5)
Absorption σ	—		$\sigma_{as} = 3 \times 10^{-25}\ m^2$
Input power	$P_p(0) = 0$–10 mW (Fig. 4) $= 0$–5 mW (Fig. 5)		$P_s(0) = 100$ nW (Fig. 4) $= 50\ \mu$W (Fig. 5)

Er^{3+} diffusing into the cladding. Larger b places ions in the low intensity portion of the pump profile, causing the amplifier to have a softer knee while approaching its peak gain. Also, the amplifier noise worsens slightly, especially in the backward direction. However, for $P_p > 5$ mW, there is no substantial difference in the small-signal gain and noise power over the range $0.6\ \mu m \leq b \leq 1.8\ \mu m$. Incidentally, by setting $\Delta\nu_k = 0$, one finds that the threshold and peak-gain coefficient are unaffected by self saturation on the ASE, but it does slow down the approach to maximum gain for $G \gtrsim 30$ dB.

The optimum amplifier length for maximum gain can be calculated from the spatial model. If the amplifier is too long, some portion of the fiber will be pumped below the inversion threshold and reabsorb the signal. A short amplifier may absorb too little of the pump power. The optimum length L_{opt} increases with pump power and decreases with the signal power. Fig. 5 shows an example of the length dependence on pump power calculated for a forward propagating signal in the absence of ASE. The optimum length is 0 m when the pump power is below the threshold pump power to achieve transparency P_{th} =

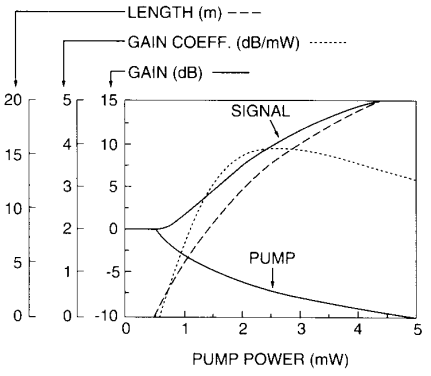

Fig. 5. Amplifier gain, gain coefficient, and length versus pump power calculated from spatial model with the length optimized to maximize gain.

$(h\nu_p A/(\sigma_{ap} + \sigma_{ep})\tau)\,(\sigma_{as}/\sigma_{es})$. As seen in Fig. 5, high-gain coefficients are obtained in moderate gain amplifiers, having $P_p(0) \gg P_{th}$, and also amplifying small input signals where most of the pump power is converted into signal.

V. Numerical Modeling of Spectral Properties

Modeling the wavelength-dependent properties of erbium-amplifiers is required in order to predict the saturation and crosstalk effects in wavelength multiplexed signals, and the behavior of the ASE spectrum. Unlike the previous spatial model where the ASE was approximated as a single optical beam, here the ASE spectrum is fully resolved and changes with pump power or saturation are described [42].

In most spectral models, the spatial mode characteristics are integrated and manifest as one parameter, the effective overlap integral. This is complementary to the spatial-mode model where the spectrum was integrated, and the spatial dimensions were resolved. Typically the spatial models are used to design the waveguide and doping parameters of the fiber, while the spectral models are used to characterize the amplifier performance.

We begin by deriving expressions for the overlap between the optical modes and the n_1, n_2 populations, in order to simplify the rate and propagation equations. Assuming that the erbium ion distribution is radially symmetric and decreases monotonically from $r = 0$, the equivalent radius of the doped region is

$$b_{\text{eff}} = \left[\frac{1}{2}\int_0^\infty \frac{n_t(r)}{n_t(0)}\, r\, dr\, d\phi\right]^{1/2} \tag{15}$$

and the average density is

$$\bar{n}_i(z) = \frac{\int_0^{2\pi}\int_0^\infty n_i(r, \phi, z) r\, dr\, d\phi}{\pi b_{\text{eff}}^2} \qquad i = 1, 2, t. \tag{16}$$

For the uniform dopant profile, $\bar{n}_t = n_t(0)$ and $b = b_{\text{eff}}$. We define the overlap integral of the n_1 and n_2 populations to be

$$\Gamma_{k,i}(z) = \frac{\int_0^{2\pi}\int_0^\infty i_k(r, \phi) n_i(r, \phi, z) r\, dr\, d\phi}{\bar{n}_i}. \tag{17}$$

Initially, the indexes on the overlap integrals for the n_1 and n_2 populations are retained, because generally they are unequal and depend on the optical power in the fiber. Next, both sides of the rate equations are integrated over the fiber core and divided by the effective area, and from the definitions of $\Gamma_{k,i}$, we find

$$\frac{d\bar{n}_2}{dt} = \sum_k \frac{P_k(z)\sigma_{ak}\Gamma_{k,1}\bar{n}_1}{h\nu_k \pi b_{\text{eff}}^2} - \sum_k \frac{P_k(z)\sigma_{ek}\Gamma_{k,2}\bar{n}_2}{h\nu_k \pi b_{\text{eff}}^2} - \frac{\bar{n}_2}{\tau}. \tag{18}$$

If the erbium ions are well confined to the center of the optical modes, then $\Gamma_{k,1}$, $\Gamma_{k,2}$ are nearly equal and replaced with a single constant Γ_k. In the Appendix, we show with a Gaussian approximation to the optical mode, $i_k = (1/\pi w^2)\exp(-r^2/w^2)$, that $\Gamma_{k,i}$ vary with P_k by less than 8% for $b < w$, corresponding to $\Gamma_{k,i} < 0.6$. After reducing the propagation equations using the effective overlap integral, our equations of the spectrally resolved, spatially integrated model become

$$\frac{\bar{n}_2}{\bar{n}_t} = \frac{\sum_k \dfrac{P_k(z)\alpha_k}{h\nu_k \zeta}}{1 + \sum_k \dfrac{P_k(z)(\alpha_k + g_k^*)}{h\nu_k \zeta}} \tag{19}$$

$$\frac{dP_k}{dz} = u_k(\alpha_k + g_k^*)\frac{\bar{n}_2}{\bar{n}_t}P_k(z) + u_k g_k^* \frac{\bar{n}_2}{\bar{n}_t} mh\nu_k \Delta\nu_k - u_k(\alpha_k + l_k)P_k. \tag{20}$$

The new fiber parameter, $\zeta = \pi b_{\text{eff}}^2 \bar{n}_t/\tau$ is the ratio of the linear density (m^{-1}) of ions to the metastable lifetime. It can be determined from measurement of the fiber saturation power P_k^{sat} as, $\zeta = P_k^{\text{sat}}(\alpha_k + g_k^*)/h\nu_k$ [43], [44]. In the effective overlap approximation, a fiber is completely characterized knowing only ζ, α_k, g_k^*, and l_k. This will be explained further with the analytical models in Sections VI and VII.

Our first example of spectral modeling is the saturation of an amplifier by two wavelength-multiplexed signals at 1545 and 1555 nm. The amplifier parameters and operating conditions are listed in Table II; features in the ASE spectrum were well resolved with $\Delta\nu_k = 125$ GHz (1 nm). This alumino-silicate glass fiber has a higher pump threshold than the fiber used in the spatial models. Calculation results are shown in Fig. 6 for equal input signal powers of either -20 or -10 dBm. At $P_{\text{in}} = -20$ dBm, the amplifier gains were 24.5 and 24.3 dB at 1545 and 1555 nm, respectively. Increasing the input powers to -10 dBm caused the gain to decrease by 4.6 dB at 1545 nm and by 3.8 dB at 1555 nm. The larger gain compression to 1545 nm due to higher ground-state absorption, illustrates the difficulty of gain equalization in WDM systems where changes in amplifier saturation alter the gain spectrum. Also, the gain saturation lowers the inversion near the output end of the amplifier, increasing the excess noise factor of the backward propagating ASE. This is seen in Fig. 6 where the backward-propagating ASE power in the saturated amplifier is 50% greater than the forward-propagating ASE.

Our next example illustrates a method of tailoring the gain spectrum by inserting an optical filter in the middle of the amplifier [45]. Unfiltered amplifiers typically have one or two peaks that are too narrow for WDM applications, and may be associated with high ASE powers that self-saturate the amplifier and reduce the pumping efficiency. Equalization of the gain spectrum can be done by placing filters at the input or output of the amplifier, but these incur either an increase in the amplifier noise figure or diminished saturated output power, respectively.

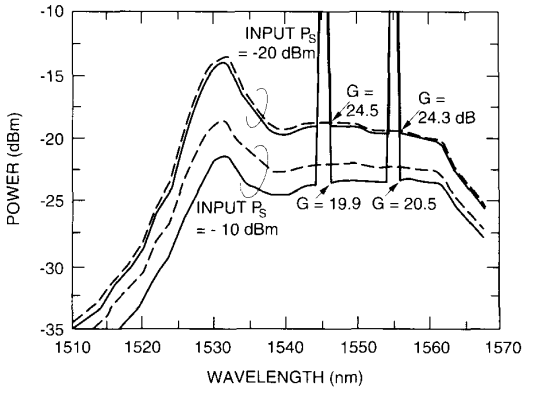

Fig. 6. Spectrally resolved calculation of two-channel amplification in a saturated amplifier. Forward (——) and backward (- - -) propagating ASE power spectra shown for 1-nm resolution.

TABLE II
FIBER PARAMETERS USED IN SPECTRAL MODEL (FIGS. 6 AND 7)

	Fig. 6	Fig. 7
Amplifier length	L = 10 m	L = 5 m
Saturation parameter	$\zeta = 4.2 \times 10^{15}\ m^{-1}\ s^{-1}$	
Pump wavelength	λ_p = 1480 nm	λ_p = 980 nm
Pump power	$P_p(0)$ = 50 mW	$P_p(0)$ = 100 mW
Signal #1 wavelength	λ_{s1} = 1545 nm	λ_{s1} = 1531 nm
Signal #2 wavelength	λ_{s2} = 1555 nm	

Placement of filters within the amplifier allow low-noise operation with high-saturated output power and equalized gain. Modeling these filters is easily achieved by adding a wavelength and z dependent loss term to propagation equation (20).

We modeled the equalization of gain for two signals at 1531 and 1550 nm in an amplifier pumped at 980 nm; the amplifier parameters are listed in Table II. Without equalization, the difference in unsaturated gain is greater than 10 dB. As seen in Fig. 7, gain equalization was achieved using a Lorentzian-shaped notch filter centered at 1531 nm, having a 3-dB bandwidth of 15 nm and minimum transmission of 5.4%. This is an absorptive filter, in order to prevent laser-cavity effects. With the filter, the small-signal gains are nearly equal, 21.6 dB at 1531 nm and 21.9 dB at 1550. Also the noise spectral density is only 1 dB higher at 1531 nm than at 1550 nm, illustrating the benefit of placing the filter in the middle of the amplifier. Better equalization over the usable gain bandwidth might be achieved with more suitably designed filter shapes.

VI. Analytical Solution to the Rate and Propagation Equations

The numerical methods just described can prevail against most of the steady-state problems of fiber amplifiers. The penalty of such generality is the loss of calculation convenience and some intuition about the amplifier behavior. For example, the notion of optimum fiber length was first posed in simple analytical form [4], and other analytical formulations for amplifier noise [46], spatial gain characteristics [47], and amplifier gain [43], [48] have appeared in the literature.

The analytical model of Saleh *et al.* [41], provides a useful comparison to the numerical solutions of the amplifier equations. Based on the assumptions that Γ_k is constant, that the amplifier is not saturated by ASE, and that excess loss is negligible, the model reduces to one implicit equation that can be solved by the Newton–Raphson technique. This model is well suited to parametric studies of the behavior of the small signal and saturated gain, optimum amplifier length, and saturated output power.

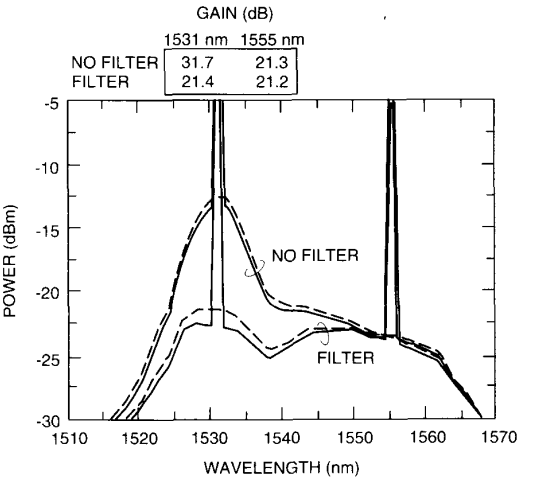

Fig. 7. Amplifier gain-leveling with an intra-amplifier bandpass filter centered at 1531 nm.

The basic equations of this model are the rate and propagation equations from which the ASE terms have been deleted. The propagation equation is

$$\frac{dP_k}{dz} = u_k\left((\alpha_k + g_k^*)\frac{\bar{n}_2}{\bar{n}_T} - \alpha_k\right)P_k \tag{21}$$

where $u_k = 1$ for forward-propagating beams, $u_k = -1$ for backward-propagating beams. Two terms on the RHS of the rate equations (18) can be replaced with (21), producing an alternate expression for the steady-state density of the metastable level

$$\bar{n}_2(z) = \frac{-\tau}{A_{\text{eff}}}\sum_j \frac{u_j}{h\nu_j}\frac{dP_j}{dz} \tag{22}$$

where $A_{\text{eff}} = \pi b_{\text{eff}}^2$. Equation (22) is substituted into (21) and after reorganizing the differentials, we find

$$\frac{dP_k}{P_k} = -u_k\left[\frac{(\alpha_k + g_k^*)}{\zeta}\sum_j \frac{u_j}{h\nu_j}\frac{dP_j}{dz} + \alpha_k\right]dz. \tag{23}$$

The two sides of this equation are integrated, so that for an amplifier length L

$$Q_k^{\text{out}} = Q_k^{\text{in}} \exp\left\{\frac{(\alpha_k + g_k^*)}{\zeta}(Q^{\text{in}} - Q^{\text{out}}) - \alpha_k L\right\}. \tag{24}$$

Here we replaced the power in the kth beam by the photon flux $Q_k = P_k/h\nu_k$, and substituted $Q^{\text{in}} = \Sigma_j\, Q_j^{\text{in}}$, $Q^{\text{out}} = \Sigma_j\, Q_j^{\text{out}}$. Summing (24) over all the k beams yields the final equation

$$Q^{\text{out}} = \sum_k Q_k^{\text{in}} \exp\left\{\frac{(\alpha_n + g_k^*)}{\zeta}(Q^{\text{in}} - Q^{\text{out}}) - \alpha_k L\right\}. \tag{25}$$

Equation (25) is an implicit equation for the total output photon flux from the amplifier, that depends only on the fiber pa-

rameters a_k, g_k^*, ζ, and L and the input fluxes Q_k^{in}. The output powers of the individual beams are obtained by solving (25) for Q^{out} and substituting it into (24).

For illustration, we apply this method to a high-efficiency amplifier fiber pumped at 1480 nm and amplifying a 1550-nm signal. This is the same fiber used in the spatial model to obtain Fig. 4(b). The saturation parameter was $\zeta = 1.5 \times 10^{15}\ m^{-1}\ s^{-1}$. First, a series of small-signal gain curves $G(P_p)$ are plotted in Fig. 8(a) for amplifier lengths varied from 5 to 20 m, and a constant input signal power of 100 nW. Comparing the 20-m amplifier calculation to Fig. 4(b) shows that this analytical model is reasonably accurate for $G \lesssim 20$ dB, before ASE saturates the amplifier gain.

An alternative presentation of the amplifier gain is to plot it as a function of length $G(L)$ for constant input pump and signal powers. These curves, plotted in Fig. 8(b), show that the optimum length yielding the maximum gain, increases with pump power. These curves become inaccurate for $G \gtrsim 20$ dB because they do not include gain saturation by ASE. Next, gain saturation at high output signal powers, is plotted in Fig. 8(c) for the 15-m long amplifier having pump powers of 1–10 mW. As expected, the saturated output power is proportional to the pump power, and at large gain compression, nearly all of the pump light is converted to signal. The last curve, Fig. 8(d), shows the pump power versus output signal power, for an amplifier length $L = 15$ m and amplifier gains of 5–25 dB. These curves help designers to determine the pump power needed for a specific amplifier gain and output signal power.

VII. Analytical Model of Amplifier Spectral Properties

The model of Saleh *et al.* accurately predicts amplifier performance from the solution of one implicit equation, using only a few easily measured amplifier parameters. With further simplification of the propagation equations under high pumping conditions, explicit equations of amplifier gain, gain saturation, and noise are derived [42]. From these, the performance limits of an amplifier, and the effects of pump and signal wavelengths are easily visualized.

The starting point for this analysis is the propagation equation written in integral form

$$G_k = \exp\left\{\int_0^L \left(g_k^* \frac{n_2}{n_t} - \alpha_k \frac{n_1}{n_t}\right) dz\right\}. \tag{26}$$

Introducing the exponential gain coefficient $g_k = \ln G_k$ and the metastable population averaged along the whole length of the amplifier, $\langle n_2 \rangle = 1/L \int_0^L n_2(z)\, dz$, we obtain

$$g_k = L\left((\alpha_k + g_k^*)\frac{\langle n_2 \rangle}{n_t} - \alpha_k\right). \tag{27}$$

From this we obtain a relationship for the wavelength dependence of the differential gain for pairs of signal (or pump) wavelengths. For two wavelengths λ_i, and λ_j, the ratio of the differential gains resulting from changes in $\langle n_2 \rangle$ is

$$\frac{dg_i}{dg_j} = \frac{g_i(\langle n_2 \rangle) - g_i(\langle n_2 \rangle + \Delta\langle n_2 \rangle)}{g_j(\langle n_2 \rangle) - g_j(\langle n_2 \rangle + \Delta\langle n_2 \rangle)} = \frac{\alpha_i + g_i^*}{\alpha_j + g_j^*}$$

$$= \frac{\Gamma_i(\sigma_{ai} + \sigma_{ei})}{\Gamma_j(\sigma_{aj} + \sigma_{ej})}. \tag{28}$$

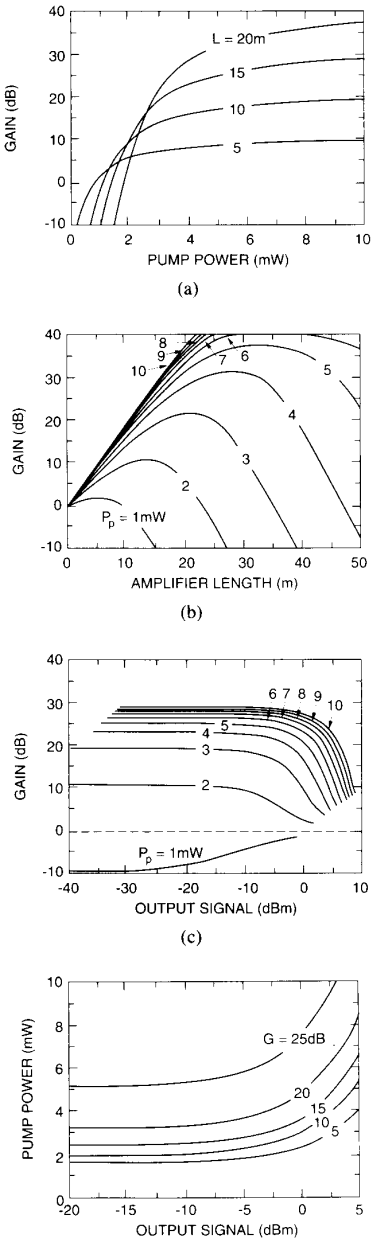

Fig. 8. Analytical computation of amplifier performance. Amplifier parameters are $\lambda_p = 1480$ nm, $\lambda_s = 1550$ nm, $\alpha(\lambda_p) = 3$ dB/m, $g^*(\lambda_p) = 1.1$ dB/m, $\alpha(\lambda_s) = 3.3$ dB/m, $g^*(\lambda_s) = 4.8$ dB/m, and $\zeta = 3 \times 10^{15}\ m^{-1}\ s^{-1}$. Figures show (a) small-signal gain versus pump power for constant length; (b) saturated gain versus output signal power for constant pump power; (c) small-signal gain versus amplifier length for constant pump power; and (d) pump power versus output signal power for constant gain.

We wrote this ratio in terms of the material absorption and emission cross sections to show that if $\Gamma_i = \Gamma_j$, then it is a function only of the glass composition, and operating temperature, and no other aspects of the amplifier design. Equation (28) explains the spectral behavior of amplifiers, including reabsorption of the gain peak at low pump powers and the prob-

lems of WDM equalization illustrated in Fig. 7. Interestingly, the differential gain equation, derived from a homogeneous gain model, predicts nonuniform gain compression in saturated amplifiers.

The differential gain equation can also be used to estimate the efficiency of converting the pump into signal in a saturated amplifier. If the total number of photons is conserved, i.e., $Q_p^{in} + Q_s^{in} = Q_p^{out} + Q_s^{out}$ then the quantum efficiency of converting the pump photons into signal photons is

$$\eta = \frac{Q_p^{in} - Q_p^{out}}{Q_p^{in}} = 1 - \exp(g_p). \tag{29}$$

Here g_p given by (27), is negative because the amplifier is absorbing the pump light.

The assumption of photon conservation implies that the spontaneously emitted light power is negligible and that the pump absorption is bleached when the signal is turned off. Consequently, the pump gain is numerically equal to its differential gain, i.e., $g_p = dg_p$, so that (28) can be substituted into (29), yielding

$$\eta = 1 - \exp\left\{-dg_s \frac{(\alpha_p + g_p^*)}{(\alpha_s + g_s^*)}\right\}. \tag{30}$$

This simple expression gives the conversion efficiency in terms of the amplifier gain compression and our usual α_k, g_k^* measured at the pump and signal wavelengths. Obviously, the conversion efficiency increases with gain saturation, and may approach unity in highly saturated amplifiers. High efficiency is achieved by designing the fiber to have a large pump overlap integral relative to that of the signal, or by using a fiber composition that maximizes $\sigma_{ap} + \sigma_{ep}/\sigma_{as} + \sigma_{es}$.

Fig. 9 shows the wavelength dependence of the amplifier efficiency for 3- and 10-dB gain compression, for pumping directly into the ${}^4I_{15/2}$-${}^4I_{13/2}$ band. The conversion efficiency is lowest around the amplifier gain peak 1530 nm because of the high absorption and emission cross sections at this signal wavelength. However, as the gain compression is increased, the effects of pump and signal wavelengths are less as η approaches unity.

Finally, we consider the noise performance limits of the erbium-doped fiber amplifier. This noise power and noise spectrum is obtained from the numerical models described earlier, or by analytical techniques. Typically, the calculations are complicated because the degree of inversion varies along the length of the amplifier and require some integration to determine the ASE power and spectrum. At high pump powers, though, the inversion is constant and equal to, $\langle n_2 \rangle / n_t = \sigma_{ap}/(\sigma_{ap} + \sigma_{ep})$. That is, the inversion is a balance between pump absorption which is filling the metastable level, and stimulated emission by the pump acting to deplete it. If the amplifier has this inversion over its entire length, then the excess noise factor n_{sp} at wavelength λ_s is

$$n_{sp} = \frac{1}{1 - \dfrac{\sigma_{ep}\sigma_{as}}{\sigma_{ap}\sigma_{es}}} = \frac{1}{1 - \dfrac{g_p^* \alpha_s}{\alpha_p g_s^*}} \tag{31}$$

and the ASE power in a bandwidth $\Delta\nu_k$ is equal to

$$P_{ASE} = 2n_{sp}(G_k - 1)h\nu_k \Delta\nu_k. \tag{32}$$

Because the amplifier is inverted uniformly n_{sp} and P_{ASE} are the same for both propagation directions. Also, for pump wavelengths where $\sigma_{ep} = 0$, complete inversion is possible and the quantum-limited noise factor $n_{sp} = 1$ can be obtained. This has been confirmed in recent measurements on amplifiers pumped at 980 nm [9].

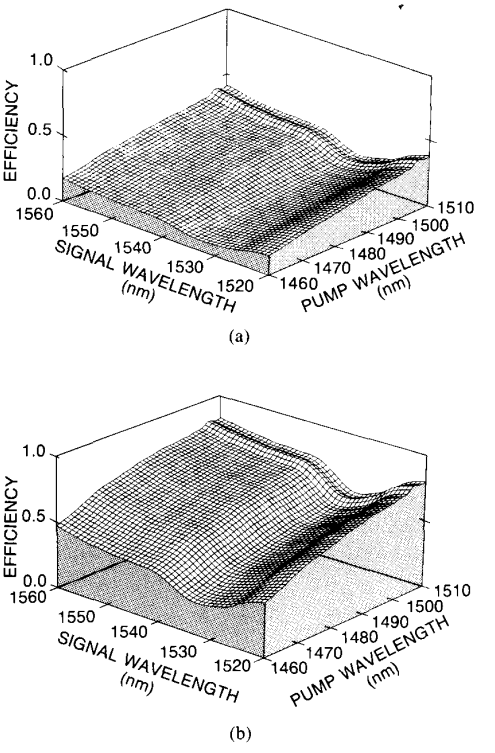

Fig. 9. Spectral dependence of pump-to-signal conversion efficiency in an Al : silicate fiber amplifier for (a) 3-dB and (b) 10-dB gain compression.

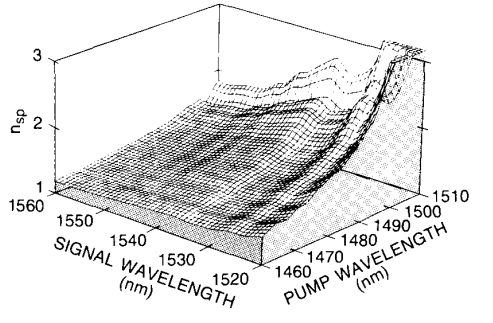

Fig. 10. Spectral dependence of noise factor in a highly pumped amplifier.

Fig. 10 shows the wavelength dependence of n_{sp} of a fiber pumped in the ${}^4I_{15/2}$-${}^4I_{13/2}$ band. Lower noise is achieved with short pump wavelengths and long signal wavelengths. If the pump wavelength is below 1487 nm, then $n_{sp} < 2$ over the signal wavelength band 1520 nm $< \lambda_s <$ 1560 nm. Low noise amplification and high pumping efficiency impose conflicting requirements on the pump wavelength. However, high efficiency is easily obtained by strongly saturating an amplifier, so the short pump wavelengths are preferred in order to lower the ASE power.

VIII. Temporal Properties of the Erbium Amplifier

While all the models discussed to this point have been for steady-state operating conditions, many applications use the erbium amplifier to amplify time-varying signals. It is well-known that the long metastable lifetime and the energy-storage properties of the gain medium act to smooth out fluctuations in the amplifier's operating point, leading to the success of these steady-state models. However, WDM transmission, analog CATV signal distribution, and high-power pulse amplification may experience signal distortion and crosstalk in amplifiers, and can only be analyzed by solutions of the time-dependent equations. Indeed, one of the first studies of the temporal properties of the erbium amplifier resorted to the numerical solution of the time-dependent rate and propagation equations [34].

For our purposes, we will examine the small-signal frequency response of the gain medium to perturbations in the pump or signal. This yields estimates of local gain fluctuations and of the limits of the validity of the steady-state models. Only the rate equation is used for this simple time-dependent problem. The optical power in the time-varying beam and the population of the metastable level are expanded about their mean value

$$P_i(t) = \bar{P}_i + \Delta P_i \exp j\omega t$$
$$n_2(t) = \bar{n}_2 + \Delta n_2 \exp j\omega t \tag{33}$$

and ΔP_i and Δn_2 are fluctuations in optical power and inversion, occurring at frequency ω. These are substituted into the rate equation and after replacing the time derivative by $d/dt = j\omega t$, we find

$$\frac{\Delta n_2}{n_t} = \frac{\dfrac{\Delta P_i}{P_i^{\text{sat}}}\left(\dfrac{P_i^{\text{sat}}}{P_i^{th}} - \sum_k \dfrac{\bar{P}_k}{P_k^{th}} \Big/ \left(1 + \sum_k \dfrac{\bar{P}_k}{P_k^{\text{sat}}}\right)\right)}{j\omega\tau + 1 + \sum_k \dfrac{\bar{P}_k}{P_k^{\text{sat}}}}. \tag{34}$$

The steady-state rate equation for n_2 and P_k was used to eliminate several terms in the expansion leading to (34). For clarity, we have introduced the threshold and saturation powers

$$P_k^{th} = \frac{h\nu_k A}{\sigma_{ak}\Gamma_k \tau} \tag{35}$$

$$P_k^{\text{sat}} = \frac{h\nu_k A}{(\sigma_{ak} + \sigma_{ek})\Gamma_k \tau}. \tag{36}$$

Apparently from (34), the local gain medium responds as a single-pole low-pass filter with a corner frequency of

$$f_c = \frac{1\left(1 + \sum_k \dfrac{\bar{P}_k}{P_k^{\text{sat}}}\right)}{2\pi\tau}. \tag{37}$$

Increasing the average power of any of the optical beams increases f_c. Frequency response measurements of amplifiers have shown typical values of $f_c \sim 5$ kHz [34], [35]. No degradation due to crosstalk was observed in WDM transmission experiments where the low-frequency content of the data was a few times higher than f_c [49], [50].

One case of interest is the perturbation of the amplifier gain caused by pump intensity noise. If we assume that the input signals are weak and the pump emission cross section is negligible, the normalized density fluctuation becomes

$$\frac{\Delta n_2}{n_t} = \frac{\Delta P_p}{\bar{P}_p} \frac{\bar{P}_p/P_p^{th}}{1 + \bar{P}_p/P_p^{th}} \frac{\exp\left\{-jA\tan\left(\omega\tau/(1 + \bar{P}_p/P_p^{th})\right)\right\}}{\left\{\omega^2\tau^2 + (1 + \bar{P}_p/P_p^{th})^2\right\}^{1/2}}. \tag{38}$$

Or in the limit of $\bar{P}_p \gg P_p^{th}$

$$\frac{\Delta n_2}{n_t} = \frac{\Delta P_p}{\bar{P}_p} \frac{\exp\left\{-jA\tan\left(\omega\tau\bar{P}_p/P_p^{th}\right)\right\}}{\left\{\omega^2\tau^2 + (\bar{P}_p/P_p^{th})^2\right\}^{1/2}} \tag{39}$$

and the dc response is

$$\frac{\Delta n_2}{n_t} = \frac{\Delta P_p P_p^{th}}{\bar{P}_p^2}. \tag{40}$$

This shows that at low frequencies, the variation in gain $\Delta g_k = \Gamma_k(\sigma_{ek} + \sigma_{ak})\Delta n_2$ is in phase with pump fluctuations. We also conclude that although the roll-off frequency increases with $\bar{P}_p$, the effects of pump noise is usually small and $\Delta g_k \ll \bar{g}_k$. Similar analysis for a time-varying signal and CW pump yields.

$$\frac{\Delta n_2}{n_t} = \frac{\Delta P_s}{P_s^{\text{sat}}}\left(\frac{P_s^{\text{sat}}}{P_s^{th}} - \frac{\bar{P}_s/P_s^{th} + \bar{P}_p/P_p^{th}}{1 + \bar{P}_s/P_s^{\text{sat}} + \bar{P}_p/P_p^{\text{sat}}}\right) \cdot \frac{\exp\left\{-jA\tan\left(\omega\tau/(1 + \bar{P}_p/P_s^{\text{sat}} + \bar{P}_p/P_p^{\text{sat}})\right)\right\}}{\left\{\omega^2\tau^2 + (1 + \bar{P}_s/P_s^{\text{sat}} + \bar{P}_p/P_p^{\text{sat}})^2\right\}^{1/2}}. \tag{41}$$

Now the low-frequency gain fluctuations are 180° out of phase with the signal, except in very underpumped amplifiers where signal absorption acts to populate the metastable level. Then the signal is attenuated rather than amplified. Again, crosstalk effects are minimized if the amplifier is strongly pumped.

IX. Summary

The homogeneous, two-level approximation of amplification in erbium-doped fibers is the basis for many amplifier models. Even three- or four-level models might be handled with modified propagation equations in the two-level model if the population densities in other levels are small. For example, in pump excited-state absorption (ESA), most of the ions are in either the metastable or ground levels; the ESA appears as a loss term in the pump propagation equation that is proportional to the metastable population. Generally then, coupled propagation equations for signal(s), pump, and ASE are integrated along the length of the amplifier while satisfying input boundary conditions. Rate equations between the population densities in the levels close the system of equations.

Left in their complete form, the propagation equations can only be solved by direct numerical integration. Often integration in the transverse or optical frequency (wavelength) coordinates is avoided to reduce the computation time. In a spatial model, integration over wavelength was replaced with an effective noise bandwidth to calculate the power in the forward and backward propagating ASE. Conversely, numerical solution to the gain and ASE spectra was done after replacing integration over the transverse coordinates with an effective overlap integral. The overlap integral should not be used if the erbium profile is larger than the optical mode spot size. Then the

propagation equations are integrated over both the transverse and frequency coordinates.

Fiber design with spatial models describes the influence of the erbium distribution inside the optical waveguide. Using a spatial model, an amplifier gain coefficient of ~ 8 dB/mW at 1480-nm pumping in small-core fibers was predicted. Other applications of spatial modeling are to analyze the effects of multimode pumping, to compare the performance of 1480- and 980-nm pumped amplifiers, and to optimize fiber design between high pump efficiency and coupling loss to transmission fibers.

Spectral modeling is used to analyze gain saturation with multiple signals and to analyze the ASE noise spectrum. Because the absorption and fluorescence spectra are different in shape, the gain spectrum changes with amplifier inversion. Then the spectral modeling is used to predict the effects of changing signal and power levels on the amplifier gain and ASE spectra. This is important for wavelength-multiplexed lightwave systems that need to maintain equal gain for each channel. Spectral modeling is also useful for studying the gain spectra of concatenated amplifier systems and the gain bandwidth reduction in multiple-stage amplifiers.

Analytical methods for modeling the amplifier gain, gain saturation, and noise have been described. Generally these are solved knowing only a few fiber parameters; the absorption and fluorescence (gain) spectra, and the ratio of the linear ion density to the metastable lifetime. Then only the amplifier length and input optical powers are needed in order to solve for the amplifier gain. Because the problem is reduced to solving a single implicit equation, it is easy to formulate the problem to optimize the amplifier design for pump efficiency and gain saturation. Also since the equation is easy to solve, this type of analytical model is suitable for a subprogram in a lightwave system model that may require numerous amplifier calculations.

Finally, analytical models describe the limiting performance of amplifier gain saturation and noise. In cases where the pump power is well above threshold, the conversion efficiency of pump into signal, and the amplifier noise factor are given by explicit equations. The effects of pump and signal wavelengths on amplifier performance are easily visualized using these models. This analysis, coupled with numerical and implicit analytical methods, enables a systematic design and performance study of erbium-doped fiber amplifiers, including multisignal amplification and ASE noise.

Appendix
Power-Dependent Overlap Integrals

The local densities of the metastable and ground levels of the erbium ions depend upon the intensities of the pump and signal beams. Consequently, the overlap integrals $\Gamma_{k,1}$, $\Gamma_{k,2}$ of (17) are functions of the optical power, and the assumption of constant Γ_k is not valid. We will check this for the case of a fiber that is uniformly doped to radius b and use the Gaussian approximation to the optical mode profile $i_k = (1/\pi w^2) \exp(-r^2/w^2)$. Considering a single optical beam, with $\sigma_{ek} = 0$, the ground-state population from the steady-state rate equation is

$$n_1(r) = \frac{n_t}{\dfrac{P_k i_k \sigma_{ak} \tau}{h\nu_k} + 1} \tag{A1}$$

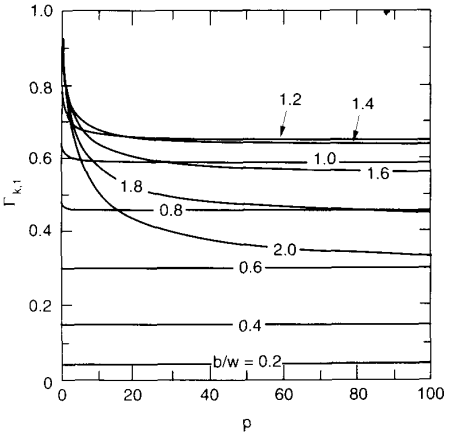

Fig. 11. Power-dependent overlap integral, $\Gamma_{k,1}$ for a Gaussian-mode approximation and an Er^{3+} distribution of $0.2 \le b/w \le 2.0$.

and the mean density n_1 over the doped core is

$$\bar{n}_1 = \frac{n_t}{\pi b^2} \int_0^{2\pi} \int_0^b \frac{1}{pe^{-r^2/w^2} + 1} r\, dr\, d\phi$$

$$= n_t \left[1 + \frac{w^2}{b^2} \ln \left(\frac{pe^{-b^2/w^2} + 1}{p + 1} \right) \right] \tag{A2}$$

where

$$p = \frac{P_k \sigma_{ak} \tau}{\pi w^2 h\nu_k}.$$

The overlap integral $\Gamma_{k,1}$ is calculated to be

$$\Gamma_{k,1} = \frac{1}{\bar{n}_1} \int_0^{2\pi} \int_0^{\infty} i_k(n) n_1(n) r\, dr\, d\phi$$

$$= \frac{-\ln \left(\dfrac{pe^{-b^2/w^2} + 1}{p + 1} \right)}{p \left\{ 1 + \dfrac{w^2}{b^2} \ln \left(\dfrac{pe^{-b^2/w^2} + 1}{p + 1} \right) \right\}}. \tag{A3}$$

Note that in the limit of $p \to 0$, $\Gamma_{k,1} = 1 - e^{-b^2/w^2}$, which is equal to $\Gamma_{k,t}$, the overlap integral between the optical mode and the total ion population.

Fig. 11 is a plot of $\Gamma_{k,1}$ versus the normalized optical power for values of b/w between 0.2 and 2. When b is much smaller than w, the optical intensity is nearly constant through the doped region. Then the n_1 distribution is uniform inside the doped region and $\Gamma_{k,1}$ is independent of the optical power. However, for $b > w$, i.e., $\Gamma_{k,1} > 0.6$, significant changes are seen. This is shown more clearly in Fig. 12 which is a plot of $F = 2[\Gamma_{k,1}(p = 0) - \Gamma_{k,1}(p \to \infty)]/[\Gamma_{k,1}(p = 0) + \Gamma_{k,1}(p \to \infty)]$, the fractional change in the overlap integral over the pump range $0 \le p < \infty$. From this, and similar results obtained for $\Gamma_{k,2}$ it looks that the constant-Γ_k approximation, which is the basis of the analytical models, can be applied with less than 8% error in Γ_k if $b < w$, $\Gamma_k < 0.6$. Otherwise the spatial mode distributions should be used to maintain the accuracy of the amplifier model.

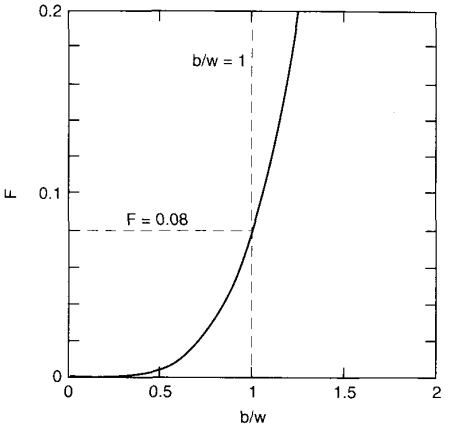

Fig. 12. Fractional change in overlap integral, $\Gamma_{k,1}$ versus b/w.

REFERENCES

[1] C. J. Koester and E. Snitzer, "Amplification in a fiber laser," *Appl. Opt.*, vol. 3, p. 1182, 1964.

[2] J. Stone and C. A. Burrus, "Neodynmium doped silica lasers in end-pumped fiber geometry," *Appl. Phys. Lett.*, vol. 23, p. 388, 1973.

[3] R. J. Mears, L. Reekie, I. M. Jauncey, and D. N. Payne, "Low noise erbium-doped fiber amplifier operating at 1.54 μm," *Electron. Lett.*, vol. 23, p. 1026, 1987.

[4] E. Desurvire, J. R. Simpson, and P. C. Becker, "High-gain erbium-doped traveling-wave fiber amplifier," *Opt. Lett.*, vol. 12, pp. 888–890, 1987.

[5] C. R. Giles, E. Desurvire, J. R. Talman, J. R. Simpson, and P. C. Becker, "2-Gbit/s signal and amplification at = λ1.53 μm in an erbium-doped single-mode fiber amplifier," *J. Lightwave Technol.*, no. 1, vol. 7, pp. 651–656, 1989.

[6] K. Hagimoto *et al.*, "A 212 km non-repeatered transmission experiment at 1.8 Gb/s using LD pumped Er^{3+}-doped fiber amplifiers in an IM/direct-detection repeater system," *OFC'89*, 1989, Paper PD15.

[7] H. Masuda and A. Takada, "High gain two-stage amplification with erbium-doped fibre amplifier," *Electron. Lett.*, vol. 26, pp. 661–662, 1990.

[8] T. Sugie, N. Ohkawa, T. Imai, and T. Ito, "An 2.5 Gb/s, 364 km CPFSK repeaterless transmission experiment employing and Er-doped fiber amplifier and SBS suppression optical link," *IEEE/LEOS Topical Meet. Optical Amplifiers* (Monterey, CA), 1990, paper PD2.

[9] W. I. Way, A. C. Von Lehman, M. J. Andrejeco, M. A. Saifi, and C. Lin, "Noise figure of a gain-saturated erbium-doped fiber amplifier pumped at 980 nm," *IEEE/LEOS Topical Meet. Optical Amplifiers* (Monterey, CA), 1990, paper TuB3.

[10] H. Nishimoto *et al.*, "Transmission of 12 Gb/s over 100 km using an LD-pumped erbium-doped fiber amplifier and a Ti:LiNbO3 Mach-Zehnder modulator," *IOOC'89* (Kobe, Japan) 1989, paper 20PDA-8.

[11] N. Edagawa *et al.*, "904 km, 1.2 Gbit/s non-regenerative optical transmission experiment using 12 Er-doped fiber amplifiers," *ECOC'89* (Gothenburg, Sweden), 1989, paper PDA-8.

[12] S. Saito *et al.*, "An over 2200 km coherent transmission experiment at 2.5 Gbit/s using erbium-doped-fiber amplifiers," *OFC'90* (San Francisco, CA), 1990, paper PD2-1.

[13] M. Nakazawa, Y. Kimura, and K. Suzuki, "An ultra-efficient erbium-doped fiber amplifier of 10.2 dB/mW at 0.98 μm pumping and 5.1 dB/mW at 1.48 μm pumping," *IEEE/LEOS Topical Meet. Optical Amplifiers* (Monterey, CA), 1990, paper PDP1.

[14] P. R. Morkel, G. Cowel, and D. N. Payne, "Single-frequency operation of a traveling-wave erbium fiber ring laser," *OFC'90* (San Francisco, CA), 1990, paper PD18.

[15] H. Avramopoulos, H. Houh, N. A. Whitaker, M. C. Gabriel, and T. Morse, "Passive mode locking of an erbium-doped fiber laser," *IEEE (LEO) Topical Meet. Optical Amplifiers* (Monterey, CA), 1990, paper PDP8.

[16] E. Eichen, W. J. Miniscalco, J. McCabe, and T. Wei, "Lossless, 2 × 2, all-fiber optical routing switch," *OFC'90* (San Francisco, CA), paper PD20.

[17] D. J. Richardson, R. I. Laming, and D. N. Payne, "Very-low threshold loop-mirror switch incorporating an EDFA," *IEEE/LEOS Topical Meet. Optical Amplifiers* (Monterey, CA), 1990, paper PDP3.

[18] P. R. Morkel and R. I. Laming, "Theoretical modeling of erbium-doped fiber amplifiers with excited-state absorption," *Opt. Lett.*, vol. 14, pp. 1062–1064, 1989.

[19] A. Bjarklev, S. L. Hansen, and J. H. Povlsen, "Large signal modeling of an erbium-doped fiber amplifier," *SPIE Conf. Fiber Laser Sources and Amplifiers* (Boston, MA), 1989, paper 1171-11.

[20] P. Urquhart and T. J. Whitley, "Long span fiber amplifiers," *Appl. Opt.*, vol. 29, pp. 3503–3509, 1990.

[21] C. R. Giles and E. Desurvire, "Propagation of signal and noise in concatenated erbium-doped fiber optical amplifiers," vol. 9, no. 2, Feb. 1991.

[22] P. Urquhart, "Review of rare earth doped fibre lasers and amplifiers," *IEE Proc.*, vol. 135, pp. 385–407, 1988.

[23] R. M. Macfarlane and R. M. Shelby, "Homogeneous line broadening of optical transitions of ions and molecules in glasses," *J. Luminescence*, vol. 36, pp. 179–207, 1987.

[24] K. Patek, "Glass Lasers," CRC Press, 1984.

[25] J. N. Sandoe, P. H. Sarkies, and S. Parke, "Variation of Er^{3+} cross-section for stimulated emission with glass composition," *J. Phys. D: Appl. Phys.*, vol. 5, pp. 1788–1799, 1972.

[26] J. G. Edwards, "Measurement of the cross-section for stimulated emission in neodymium-doped glass from the output of a free-running laser oscillator," *Brit. J. Appl. Phys.* (J. Phys. D), vol. 2, pp. 449–456, 1968.

[27] M. J. Weber, "Laser excited fluorescence spectroscopy in glass," from *Laser Spectroscopy of Solids*, W. M. Yen and P. M. Selzer, Eds. New York: Springer, 1986.

[28] A. E. Siegman, *Lasers*. University Science Books, 1986, ch. 30.

[29] E. Desurvire, J. L. Zyskind, and J. R. Simpson, "Spectral gain hole-burning at 1.53 μm in erbium-doped fiber amplifiers," *IEEE Photon. Technol. Lett.*, vol. 2, p. 246, 1990.

[30] J. L. Zyskind, E. Desurvird, J. W. Sulhoff, and D. J. DiGiovanni, "Spectral gain hole-burning in an erbium-doped fiber amplifier," *IEEE/LEOS Topical Meet. Optical Amplifiers* (Monterey, CA), 1990, paper MD4.

[31] S. Zemon, G. Lambert, W. J. Miniscalco, L. J. Andrews, and B. T. Hall, "Characterization of Er^{3+}-doped glasses by fluorescence line narrowing," *SPIE Symp. Fiber Laser Sources and Amplifiers* (Boston, MA), 1989, paper 1171-23.

[32] E. Desurvire, J. W. Sulhoff, J. L. Zyskind, and J. R. Simpson, "Spectral dependence of gain saturation and effect of inhomogeneous broadening in erbium-doped aluminosilicate fiber amplifiers," *IEEE/LEOS Topical Mtg Optical Amplifiers* (Monterey, CA), 1990, paper PD9.

[33] C. B. Layne, W. H. Lowdermilk, and M. J. Weber, "Multiphonon relaxation of rare-earth ions in oxide glasses," *Phys. Rev. B*, vol. 16, pp. 10–20, 1977.

[34] C. R. Giles, E. Desurvire, and J. R. Simpson, "Transient gain and cross talk in erbium-doped fiber amplifiers," *Opt. Lett.*, vol. 14, pp. 880–882, 1989.

[35] R. I. Laming, L. Reekie, P. R. Morkel, and D. N. Payne, "Multichannel crosstalk and pump noise characterization of Er^{3+}-doped fibre amplifier pumped at 980 nm," *Electron. Lett.*, vol. 25, pp. 455–456, 1989.

[36] D. Gloge, "Weakly guiding fibers," *Appl. Opt.*, vol. 10, pp. 2252–2257, 1971.

[37] L. B. Jeunhomme, "Single-mode fiber optics—principles and applications," Marcel Dekker, Inc., 1983.

[38] J. R. Armitage, "Three-level fiber laser amplifier: A theoretical model," *Appl. Opt.*, vol. 27, pp. 4831–4836, 1988.

[39] E. Desurvire, J. L. Zyskind, and C. R. Giles, "Design optimization for efficient erbium-doped fiber amplifiers," *J. Lightwave Technol.*, vol. 8, no. 11, pp. 1730–1741, 1990.

[40] J. R. Simpson *et al.*, "A distributed erbium-doped fiber amplifier," *Optical Fiber Conf.* (San Francisco, CA), 1990, postdeadline paper PDP19.
[41] J. L. Zyskind, D. J. DiGiovanni, J. W. Sulhoff, P. C. Becker, and C. H. Brito Cruz, "High performance erbium-doped fiber amplifier pumped at 1.48 μm and 0.97 μm," *IEEE/LEOS Topical Meet. Optical Amplifiers* (Monterey, CA), 1990, paper PDP6.
[42] E. Desurvire and J. R. Simpson, "Amplification of spontaneous emission in erbium-doped single-mode fibers," *J. Lightwave Technol.*, vol. 7, p. 835, 1989.
[43] A. A. M. Saleh, R. M. Jopson, J. D. Evankow, and J. Aspell, "Modeling of gain in erbium-doped fiber amplifiers," *IEEE Photon. Technol. Lett.*, Oct. 1990.
[44] C. R. Giles and D. DiGiovanni, "Spectral dependence of gain and noise in erbium-doped fiber amplifiers," *Photon. Technol., Lett.*, vol. 2, no. 11, pp. 797–800, 1990.
[45] M. Tachibana, R. I. Laming, P. R. Morkel, and D. N. Payne, "Gain-shaped erbium-doped fibre amplifier (EDFA) with broad spectral bandwidth," *IEEE/LEOS Topical Meet. Optical Amplifiers* (Monterey, CA), 1990, paper MD1.
[46] R. Olshansky, "Noise figure for erbium-doped optical fibre amplifiers," *Electron. Lett.*, vol. 24, pp. 1363–1365, 1988.
[47] J. R. Armitage, "Spectral dependence of the small-signal gain around 1.5 μm in erbium doped silica fiber amplifiers," *IEEE J. Quantum Electron.*, vol. 26, pp. 423–425, 1990.
[48] M. Peroni and M. Tamburrini, "Gain in erbium-doped fiber amplifiers: A simple analytical solution to the rate equations," *Opt. Lett.*, vol. 15, pp. 842–844, 1990.
[49] E. Desurvire, C. R. Giles, and J. R. Simpson, "Gain saturation effects in high-speed, multichannel erbium-doped fiber amplifiers at =1.53 μm," *J. Lightwave Technol.*, vol. 7, pp. 2095–2104, 1989.
[50] K. Inoue, H. Toba, N. Shibata, K. Iwatsuki, and A. Takada, "Mutual signal gain saturation in Er^{3+}-doped fibre amplifier around 1.54 μm wavelength," *Electron. Lett.*, vol. 25, pp. 594–595, 1989.

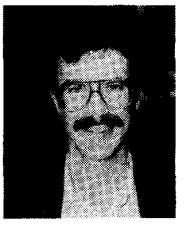

C. Randy Giles (M'88) was born in Vancouver, Canada, on May 8, 1955. He received the B.Sc. and M.Sc. degrees in physics from the University of Victoria, Victoria, B.C., in 1976 and 1978, respectively, and the Ph.D. degree in electrical engineering from the University of Alberta, Edmonton, in 1983.

From 1983 to 1983 he worked at Bell Northern Research, Canada, on high-speed lightwave systems and the modulation properties of semiconductor lasers. In 1986 he joined AT&T Bell Laboratories and has engaged in research on integrated-optic devices and fiber optical amplifiers.

Dr. Giles is a member of the Optical Society of America.

*

Emmanuel Desurvire (M'89) received the M.S. degree in physics in 1980 and the Diplôme d'Etudes Approfondies in theoretical physics in 1981, from the University of Paris VI. In 1983, he received the Doctorat de Troisième Cycle in Physics from the University of Nice, France. His doctoral work involved the study of Raman fiber amplifiers.

He then spent two years at a Postdoctoral Research Affiliate at the E. L. Ginzton Laboratory, Stanford University, working on the implementation of Raman amplification to recirculating fiber delay lines and reentrant fiber gyroscopes. From 1986 to 1990, he has been with AT&T Bell Laboratories at Crawford Hill, NJ, working on erbium-doped fiber amplifiers and applications to optical communication systems. He is now Associate Profesor in the Electrcal Engineering Department at Columbia University.